Rodolfo T. Gonçalves[1]
OSPL—Ocean Space Planning Laboratory,
Department of Systems Innovation,
School of Engineering,
The University of Tokyo,
Bunkyo-ku, Tokyo 113-8656, Japan
e-mail: goncalves@g.ecc.u-tokyo.ac.jp

Edgard B. Malta
Technomar Engenharia Oceânica,
São Paulo, SP 03178-200, Brazil
e-mail: edgard@technomar.com.br

Alexandre N. Simos
TPN—Numerical Offshore Tank Laboratory,
Department of Naval Architecture and Ocean Engineering,
Escola Politécnica, University of São Paulo,
São Paulo, SP 05508-030, Brazil
e-mail: alesimos@usp.br

Shinichiro Hirabayashi
OSPL—Ocean Space Planning Laboratory,
Department of Ocean Technology, Policy, and Environment,
School of Frontier Sciences,
The University of Tokyo,
Kashiwa-shi, Chiba 277-0882, Japan
e-mail: hirabayashi@k.u-tokyo.ac.jp

Hideyuki Suzuki
OSPL—Ocean Space Planning Laboratory,
Department of Systems Innovation,
School of Engineering,
The University of Tokyo,
Bunkyo-ku, Tokyo 113-8656, Japan
e-mail: suzukih@sys.t.u-tokyo.ac.jp

Influence of Heave Plate on the Flow-Induced Motions of a Floating Offshore Wind Turbine

Flow-induce motions (FIM) small-scale model tests were performed for the Jappaku floating offshore wind turbines (JPK), a FOWT developed to operate in Brazilian waters. This paper aims to investigate the presence of FIM on the JPK to show the importance of heave plate (HP) design and to show how HP mitigates FIM. Three different HP dimensions were tested and compared with the condition without HP. In addition, two different incidence angles of the current were tested, namely, 0 deg and 180 deg. The results showed amplitudes in the transverse direction similar to the diameter of the external platform column for the case without HP. These amplitudes are higher than the ones observed for previous deep-draft semi-submersibles found in the literature. Conversely, the largest HP dimensions implied in mitigation of the FIM amplitudes, i.e., very low amplitudes, were observed. The presence of the central column played an essential role in FIM and significantly modified the amplitudes in different current incidences. Due to the different diameters of the external and central columns, the FIM presented two different branches of response related to the vortex-shedding frequency around the columns. The results showed that significant FIM could occur for this specific JPK investigation even with HP. The HP design has a positive effect on reducing dynamic behaviors due to the wave and current incidences. Therefore, its design must be included in the preliminary stages of FOWT developments.
[DOI: 10.1115/1.4056345]

Keywords: flow-induced motions (FIM), floating offshore wind turbines (FOWT), model tests, design of offshore structures, fluid–structure interaction, vortex-induced vibration

1 Introduction

Flow-induced motions (FIM) are an issue for multi-column platforms, such as Floating Offshore Wind Turbines (FOWT). The phenomenon can increase the fatigue failure of the mooring and/or cable systems and can also stop the turbine operation. Differently from the high-frequency structural damage due to the wave-induced motions (WIM), the FIM causes a low-frequency structural damage.

As pointed out by Blevins [1] and Zhao et al. [2], non-symmetric bluff bodies, for example, multi-column systems, are susceptible to two main FIM: vortex-induced motions (VIM), where the frequency of periodic vortex shedding and the frequency of the body oscillation synchronize; and galloping, an aeroelastic instability, caused by changes in the relative angle of attack induced by the body motion resulting in aerodynamic forces in the same degree-of-freedom (DOF) as the motion.

Since the new projects reach large dimensions of single and multi-column systems, these systems are exposed to the ocean environment as current incidence, and they are subject to FIM amplitudes, an extensive state-of-art review can be found in the study by Yin et al. [3]. In addition, new FOWTs have demanded dimension changes to meet the turbine limits of working time, such as the acceleration of the nacelle of the rotor and inclination angles of the tower [4].

Different FOWT platform configurations have been studied, as by Liu et al. [5], Lemmer et al. [6], Suzuki et al. [7], and Mello et al. [8]. However, few works addressing the FIM phenomenon of FOWT could be found in the literature; the ones encountered were reported by Carlson and Sadeghi [9] and Gonçalves et al. [10] for a single and multi-column configuration, respectively.

One of the solutions to reduce the wave-induced motions (WIM) of FOWT designs is the inclusion of heave plates (HP). The heave plate is a flat structure attached to the column bottom aiming to increase the added mass and damping of the system, and consequently, the usage of HP mainly decreases the vertical response in waves of the FOWT; however, the behavior was not deeply investigated in the presence of currents.

The benchmarking FOWT semi-submersible type (OC4 phase II) presents HPs to improve the hydrodynamic behavior, as in the study by Robertson et al. [11]. Studies by Lopez-Pavon and Souto-Iglesias [12], Thiagarajan and Moreno [13], Jiang et al. [14], and Takta et al. [15] showed HP as a good solution for multi-column FOWT. Kosasih et al. [16] conducted studies of a barge-type FOWT that presented heave plates to minimize the wave effects in the vertical motions. Moreover, fundamental studies about heave plate effects on added mass, damping, and FIM can be found for a single-column platform in Gonçalves et al. [17].

In the study by Mello et al. [8], an analysis of heave plates to improve the FOWT performance in waves was presented. The work was developed for designing a FOWT to operate in Brazilian

[1]Corresponding author.

Contributed by the Ocean, Offshore, and Arctic Engineering Division of ASME for publication in the Journal of Offshore Mechanics and Arctic Engineering. Manuscript received August 19, 2022; final manuscript received November 16, 2022; published online December 26, 2022. Assoc. Editor: Madjid Karimirad.

waters, Jappaku FOWT (JPK). The multi-column system contains four vertical columns. Heave plates were positioned at the bottom of each column, and the use of heave plate height was analyzed to help tune the natural periods in heave, roll, and pitch without further increasing the diameter of the plates. A combination of three heave plate diameters, D_p, and three heave plate heights, H_p, were studied. Decay tests for heave, pitch, and surge were performed to evaluate the added mass and damping levels. Further, regular and irregular wave tests were performed to validate a numerical model using the potential theory.

Following the same geometry parameters investigated by Mello et al. [8], the present work aims to examine the effect of the heave plate geometry subject to the incidence current and, consequently, the FIM amplitudes of the JPK. Results regarding FIM amplitudes in the transverse and yaw motion directions are presented for each configuration.

2 Experimental Setup

The experimental tests were performed in the towing tank at the University of Tokyo (Japan). Regarding the main dimensions, the towing tank facility has 85 m in length, 3.5 m in width, and 2.4 m in depth.

The JPK model is based on the JPK definition as presented in Fig. 1 and described by Mello et al. [8]. The reduced-scale model has a scale of 1:60 based on Froude scaling, and details are presented in Table 1. Figure 2 contains the main parameters of the platform; Fig. 3 presents the picture of the reduced-scale model used during the experiments.

The reduced-scale model was connected to four linear springs attached to the towing carriage, as shown in Fig. 4. The simplified mooring system can be considered linear for the range of the displacements observed during the experiments, as calculated by applying the analytical formulation by Pesce et al. [18].

A deck made of acrylic was constructed to attach the mooring system and support the passive targets used for the motion-capturing device. The deck configuration allowed the current incident angle changes, keeping the same restoring force. Each mooring line presented a stiffness of 7.6 N/m and 9.4 N/m, with

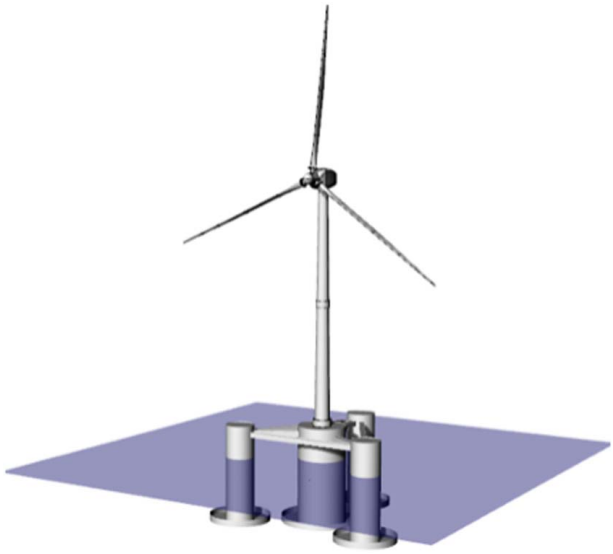

Fig. 1 Jappaku FOWT (JPK) 3D model

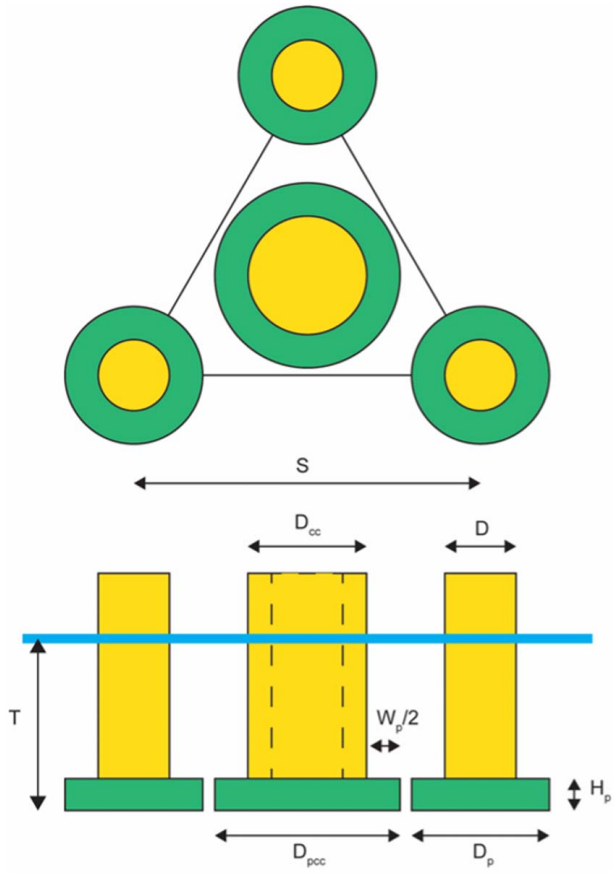

Fig. 2 Model parameters

Table 1 Main dimensions of the JPK models tested

Property	HP0	HPS	HPM	HPL
T (mm)		333.0		
S (mm)		733.3		
D (mm)		150.0		
D_{cc} (mm)		250.0		
W_p (mm)	0.0	140.0	170.0	200.0
H_p (mm)	0.0	70.0	85.0	100.0
D_p (mm)	0.0	290.0	320.0	350.0
D_{pcc} (mm)	0.0	390.0	420.0	450.0
m (kg)	34.04	41.09	42.55	44.47

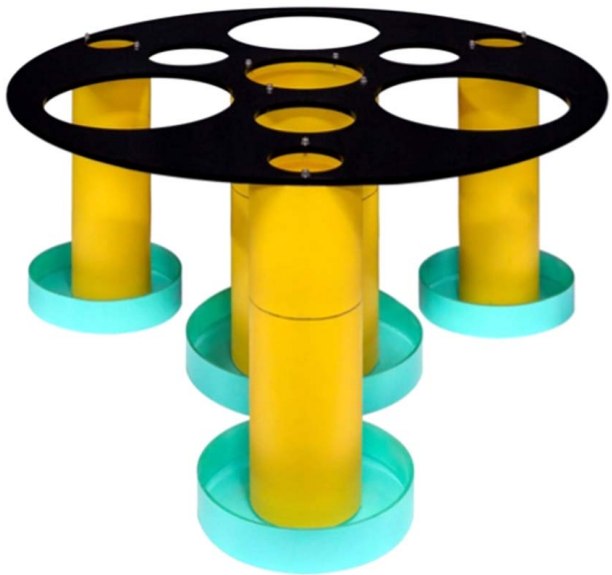

Fig. 3 Picture of the 1:60 reduced-scale model of the JPK

pre-tension equal to 9.0 N and 8.2 N for inline and transverse directions, respectively. The total stiffness in the inline, transverse, and yaw directions were $K_X = 30.1$ N/m, $K_Y = 28.3$ N/m, and $K_{yaw} = 0.51$ N · m/deg, respectively.

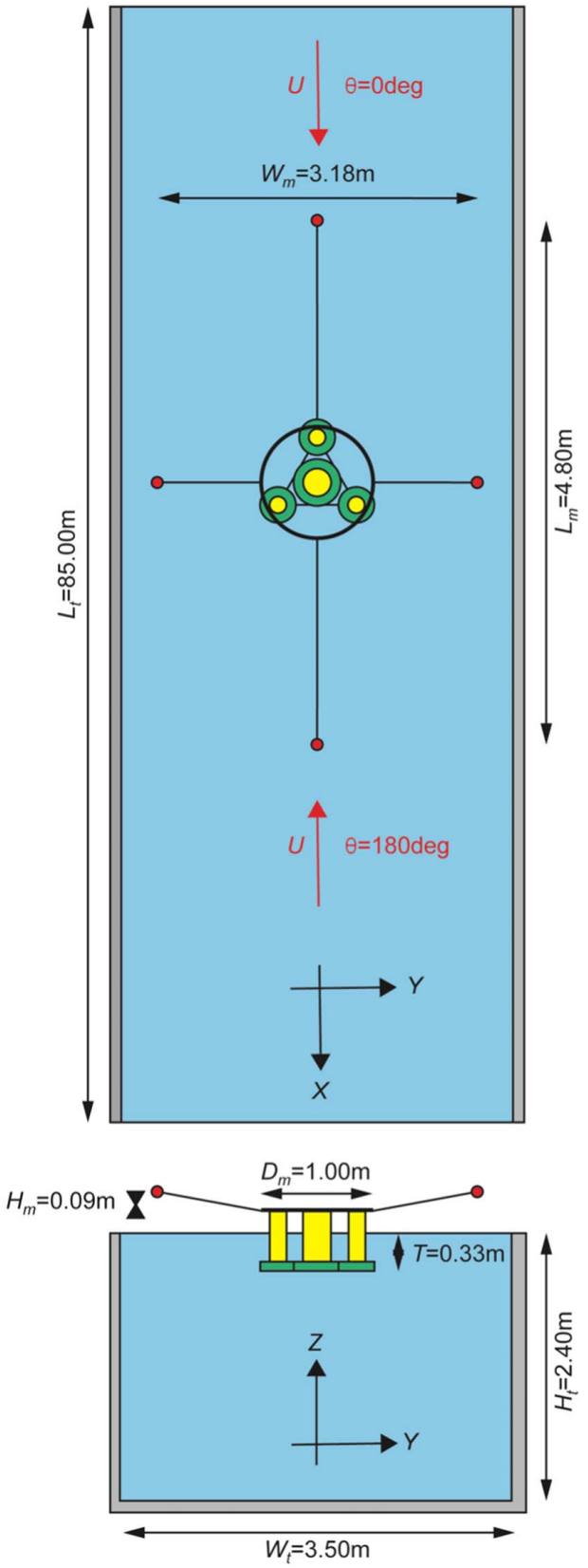

Fig. 4 Sketch of the simplified mooring system setup composed of four spring lines at the towing tank

Table 2 Natural periods damping obtained from decay tests in still water for the different heave plate dimensions

Degree-of-freedom	HP0	HPS	HPM	HPL
T_{0X} (s)	9.14 ± 0.01	10.21 ± 0.05	10.51 ± 0.04	11.06 ± 0.02
T_{0Y} (s)	9.76 ± 0.02	10.66 ± 0.01	11.08 ± 0.03	11.58 ± 0.02
T_{0Z} (s)	1.26 ± 0.01	1.95 ± 0.01	2.20 ± 0.01	2.55 ± 0.01
T_{0pitch} (s)	1.83 ± 0.01	2.56 ± 0.01	2.75 ± 0.02	2.99 ± 0.01
T_{0yaw} (s)	3.52 ± 0.01	3.88 ± 0.01	4.01 ± 0.01	4.21 ± 0.01

The HP considered has only a bottom side forming an L-shaped cross section, as defined in the JPK model by Mello et al. [8]. The HP dimensions were modified to verify the HP effects on the FIM of the JPK model. As proposed by Mello et al. [8], the ratio between the width and height of the plates was kept constant as $W_p/H_p = 2$. The ratio between the HP width and the characteristic diameter, in this case, chosen as the diameter of the external columns, D, was modified as $W_p/D = 0.48$, 0.53, and 0.57, respectively, named as HPS, HPM, and HPL cases. The case without the HP was called HP0.

The draft of the JPK models was kept constant during the experiments, i.e., $T = 330$ mm, which corresponds to a column aspect ratio, $T/D = 2.2$.

The natural periods, T_{0n}, and linear damping, ζ_n, obtained during the decay tests in still water are presented in Table 2 and, respectively, where n represents the corresponding DOF.

The 6DOFs platform motions were measured using an optical motion capturing system (Qualisys®) composed of four cameras and five passive targets attached to the model deck. Those measurements were acquired at a sampling frequency of 100 Hz.

Two main incidence angles were tested, particularly 0 deg and 180 deg, as described in Fig. 4. For each incidence angle, at least 25 reduced velocities were carried out. The uniform current profile was simulated by towing the model supported by the towing car.

The range of the incident current velocity, or towing car velocity, was $0.05 \text{ m/s} \leq U \leq 0.30$ m/s. Each VIM run was performed along the 60-m length of the towing tank; therefore, the time duration of each run depended on U. More than ten cycles in a steady-state were carried out in each run, and it was considered enough to provide reliable statistical results. No repetition for each run was performed following the methodology proposed by Gonçalves et al. [10], which guarantees confident results.

Figure 5 shows an example of time series of the non-dimensional in-line and transverse displacements. From 0 s to 60 s, the transient region comprises the time of the car acceleration to the tested incidence current velocity and the time to achieve the model equilibrium drift position. The steady-state phenomenon is considered from 60 s to the end of the run characterized by the end of the towing tank, i.e., the limit of the measurements.

3 Analysis Methodology

3.1 Reduced Velocity. The reduced velocity V_r is defined as a function of the incident current velocity, U, the natural period of the motion in the transverse direction in still water, T_{0Y}, and the characteristic length of the body section subjected to vortex shedding, D. The characteristic length was defined as the diameter of the external columns, D, thus

$$V_r = \frac{U.T_{0Y}}{D} \tag{1}$$

In this case, the range of $4 < V_r < 25$ was tested.

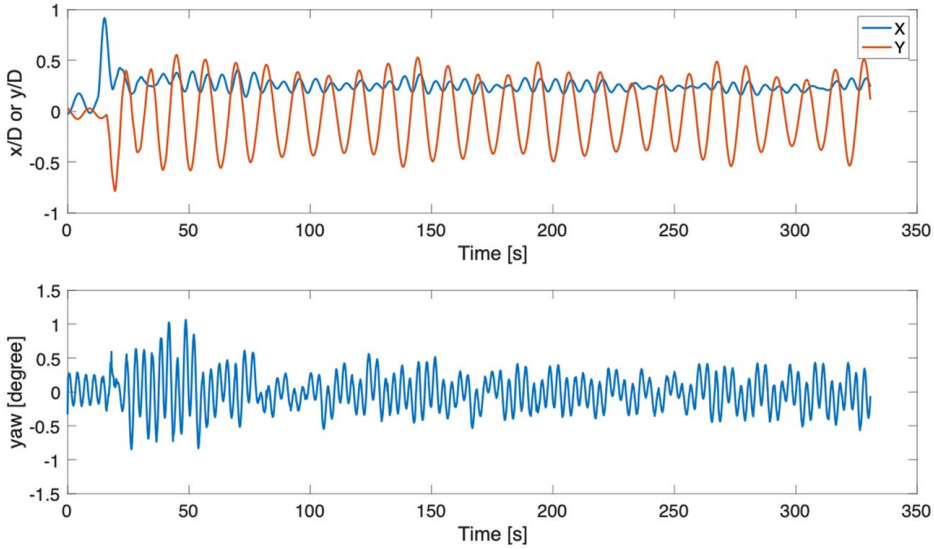

Fig. 5 Time histories of the VIM test of non-dimensional in-line, transverse, and yaw displacements for HP0, $\theta = 0$, and $U = 0.09$ m/s condition

3.2 Reynolds Number. The Reynolds Number Re is defined as below, where ν is the kinematic viscosity of the fluid.

$$\mathrm{Re} = \frac{UD}{\nu} \tag{2}$$

Here, the range of $7{,}000 < \mathrm{Re} < 50{,}000$ was tested.

3.3 Motion Amplitudes. Motions in the 6DOFs were measured. The FIM response of the JPK model was analyzed through the root-mean-square (RMS) of the displacements, considering a signal of a zero mean, in the inline and transverse directions and angles of rotation in the case of the yaw motion. The RMS was calculated in the case of a set of n values (x_1, x_2, …, x_n) as

$$x_{RMS} = \sqrt{\frac{1}{n}.(x_1^2 + x_2^2 + \ldots + x_n^2)} \tag{3}$$

Moreover, as commonly found, non-dimensional characteristic amplitudes in the in-line direction were calculated as a quotient of the RMS displacements, A_Y, by the diameter of the external columns, D, and multiplied by $\sqrt{2}$, thus

$$\frac{A_Y}{D} = \frac{\sqrt{2} y_{RMS}}{D} \tag{4}$$

The same procedure was applied to the transverse and vertical directions. For the characteristic amplitude of the roll, pitch, and yaw angles, no dimensionless form was adopted, for example

$$A_{yaw} = \sqrt{2} yaw_{RMS} \tag{5}$$

4 Experimental Results

In this section, the results of the analysis of the FIM phenomenon of the FOWT based on the JPK model are presented concerning two different angles of the current incidence, namely, 0 and 180 deg. The results are compared for three HP dimensions and the case without HP as a reference. Finally, the discussion addresses the HP effects and the central column presence.

Figures 6 and 7 present the results of the non-dimensional nominal amplitudes of the motions in the transverse direction, A_Y/D, for 0- and 180-deg incidences, respectively. As expected, the highest values of A_Y/D were observed for the case without the HP.

A_Y/D decreased when increasing the HP dimensions. However, for the smallest HP, $W_p/D = 0.48$, it is still possible to observe

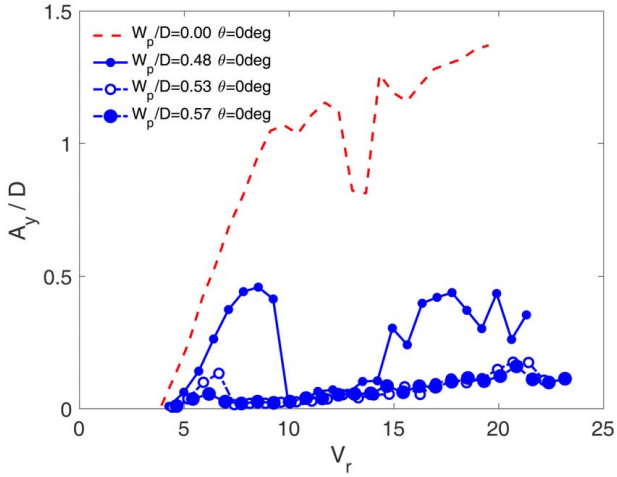

Fig. 6 Non-dimensional nominal amplitudes of the motions in the transverse direction for the JPK model with 0-deg incidence and different HP dimensions

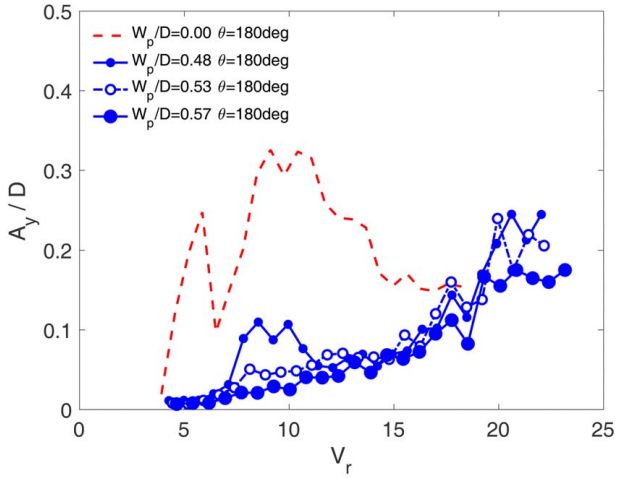

Fig. 7 Non-dimensional nominal amplitudes of the motions in the transverse direction for the JPK model with 180-deg incidence and different HP dimensions

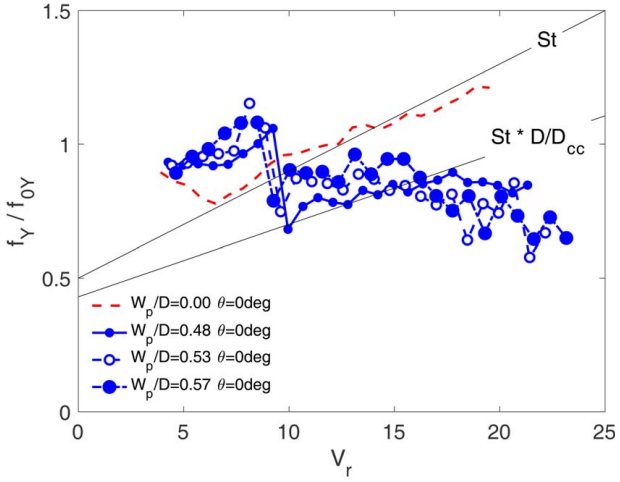

Fig. 8 Non-dimensional frequency for the motions in the transverse direction for the JPK model with 0-deg incidence and different HP dimensions

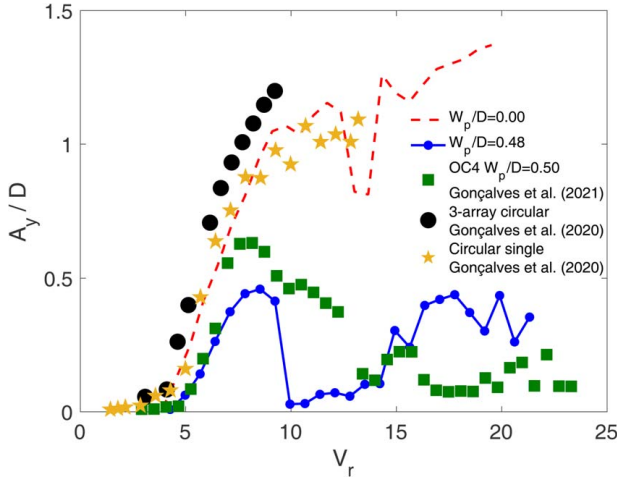

Fig. 10 Comparison of non-dimensional nominal amplitudes of the motions in the transverse direction for model tests of different geometries of platforms with 0-deg incidence

high FIM amplitudes around 50% of the characteristic diameter, a value similar to those surveyed for DD-SS. Moreover, the FIM phenomenon was mitigated for larger HP dimensions, $W_p/D > 0.48$.

A significant difference in A_Y/D can be observed when comparing the same HP dimension and different current incidences. The further wake disturbance can explain this behavior due to the multicolumn geometry. In addition, the wakes interact with each other differently due to the current incidence angle.

In the wake formation and vortex shedding, the central column played an essential role due to its larger diameter than the external columns. For example, the downstream external column was totally immersed in the wake due to the upstream central column for the 180-deg incidence. Therefore, the total force of the system was modified and resulted in different FIM amplitudes.

The increase in amplitudes when increasing the reduced velocity, mainly for 180-deg incidence, may occur due to a "galloping-like behavior." The source of the "galloping-like behavior" of the motion results may be related to the WIV—wake-induced vibration. As pointed out by Assi [19], when a bluff body, like a circular cylinder, is immersed in the wake developed from an upstream body, it will dynamically respond with wake-induced vibrations (WIVs). This mechanism has also been referred to as "wake-induced galloping," "interference galloping," or "wake-displacement excitation."

Figures 8 and 9 present the results of the non-dimensional dominant frequency for the motions in the transverse direction, f_Y/f_{0Y}, for 0- and 180-deg incidences, respectively. Again, it is possible to observe two different behaviors. One behavior occurred for $V_r < 10$, related to synchronization associated with a predominant vortex shedding around the outside columns. Consequently, the other behavior for $V_r > 10$ was associated with the predominant vortex shedding of the central column.

When drawing a Strouhal-like number curve, as proposed by Gonçalves et al. [20], using $\mathrm{St} = f_y D/U$, it appeared to two distinct St determined by the curve slope. Considering that St was constant for each column, it may explain the two different synchronization regions due to the two distinct column diameters. In the second region, the new slope curve followed the expression $\mathrm{St}D/D_{cc}$. This behavior was pronounced for the 180-deg incidence, whereby the central column played an important role.

The FIM results of A_Y/D can be compared for different multicolumn platforms to better understand the effect of the central column presence and current incidence angle. Figures 10 and 11 present a result comparison of A_Y/D for different platform geometries with 0- and 180-deg incidence angles, respectively. The present study without HP, $W_p/D = 0.48$, and $T/D = 2.22$ was compared with the results of a single-cylinder case without HP [21]; a three-circular-cylinder array without the presence of a

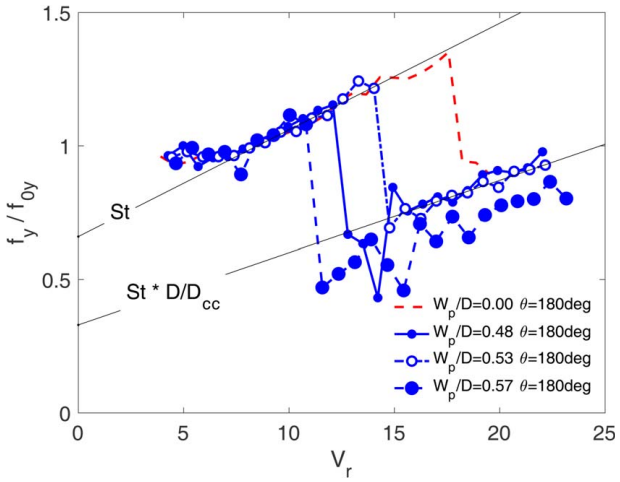

Fig. 9 Non-dimensional frequency for the motions in the transverse direction for the JPK model with 180-deg incidence and different HP dimensions

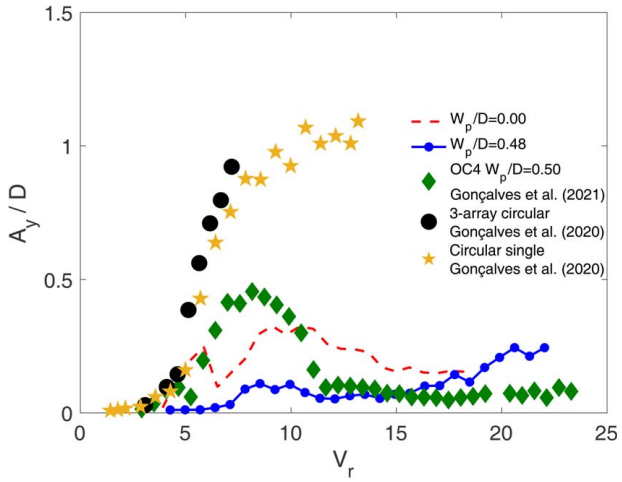

Fig. 11 Comparison of non-dimensional nominal amplitudes of the motions in the transverse direction for model tests of different geometries of platforms with 180-deg incidence

Table 3 Linear hydrodynamic damping obtained from decay tests in still water for the different heave plate dimensions

Property	HP0	HPS	HPM	HPL
ζ_X (%)	3.38 ± 0.14	4.76 ± 0.27	5.99 ± 0.33	6.09 ± 0.07
ζ_Y (%)	3.18 ± 0.24	4.62 ± 0.13	5.38 ± 0.25	5.73 ± 0.39
ζ_Z (%)	3.74 ± 0.34	4.52 ± 0.10	4.79 ± 0.09	5.11 ± 0.20
ζ_{pitch} (%)	2.45 ± 0.23	4.70 ± 0.14	4.92 ± 0.18	4.34 ± 0.34
ζ_{yaw} (%)	2.62 ± 0.05	4.85 ± 0.16	5.20 ± 0.20	6.03 ± 0.31

central column and HP and $T/D = 1.50$ [21,22]; and then compared with the OC4 FOWT that presents an HP, $W_p/D = 0.50$, $T/D = 1.64$, and a small circular central column [10].

In Fig. 10, A_Y/D results showed that the presence of the central columns was less critical than the presence of HP. The cases of a single circular cylinder, an array of three cylinders, and the present case with $W_p/D = 0.48$ presented the same behavior for $V_r < 10$. On the other hand, the presence of HP decreased the A_Y/D, and it was accentuated for the present case, whereby the column diameter ratio was $D_{cc}/D = 1.67$ instead of $D_{cc}/D = 0.55$ for the OC4 case. This is because the OC4 floater has thick heave plates with top and bottom sides, whereas HP forms an L-shaped cross section. The difference between HP may impact different levels of damping and added mass as shown in Tables 2 and 3.

The values of the column aspect ratio, T/D, ranged from 1.5 for the array of three cylinders up to 2.22 for the present cases. The OC4 model presented $T/D = 1.64$. As pointed out by Gonçalves et al. [20], single cylinders with low aspect ratio with $1.5 < T/D = 2.00$ did not present a significant change in the amplitudes due to the vortex shedding. Therefore, a coupled effect between HP and central column configurations was responsible for the different amplitudes of OC4 and present cases.

In Fig. 11, the effect of the incidence is evident for the case with HP and central columns. The incidence angle was not a role for an array of three cylinders since the amplitudes were similar for the 0- and 180-deg incidences. As stated by Gonçalves et al. [22], for circular cases with center column distances larger than three diameters, the behavior was similar for the single-cylinder case; i.e., the wake interference in those cases was weak.

Comparing the same conditions for 0- and 180-deg incidence with HP and central columns, it was possible to see significant differences in the present work and in the OC4 case. Comparing the present case with and without HP, only the current incidence angle decreased the transverse amplitudes. In this case, the presence of the central column was responsible for interfering with the wake and vortex shedding, which implied a different FIM behavior.

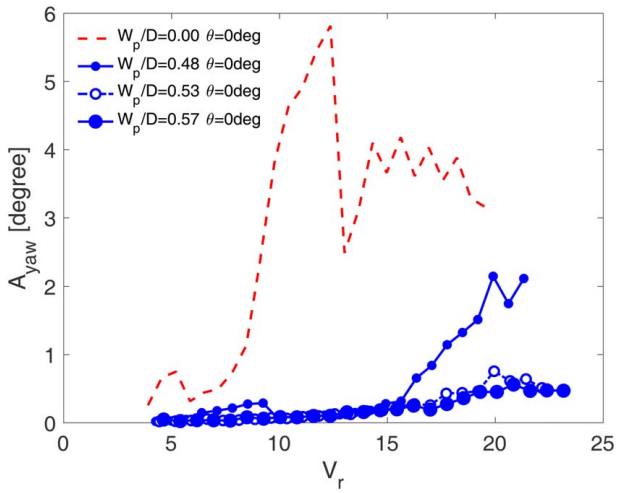

Fig. 12 Non-dimensional nominal yaw motion amplitudes for the JPK model with 0-deg incidence and different HP dimensions

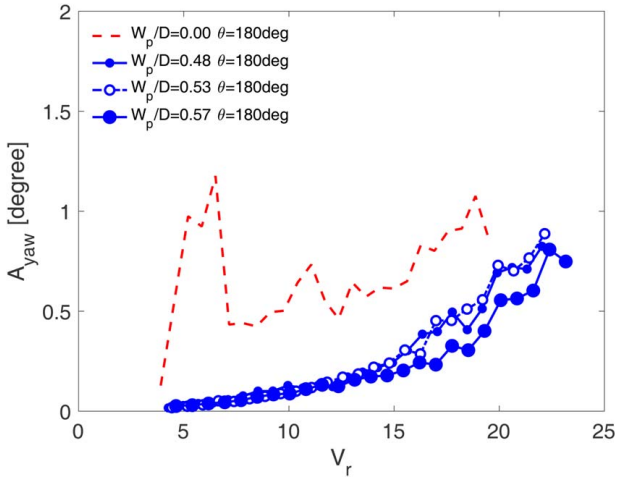

Fig. 13 Non-dimensional nominal yaw motion amplitudes for the JPK model with 180-deg incidence and different HP dimensions

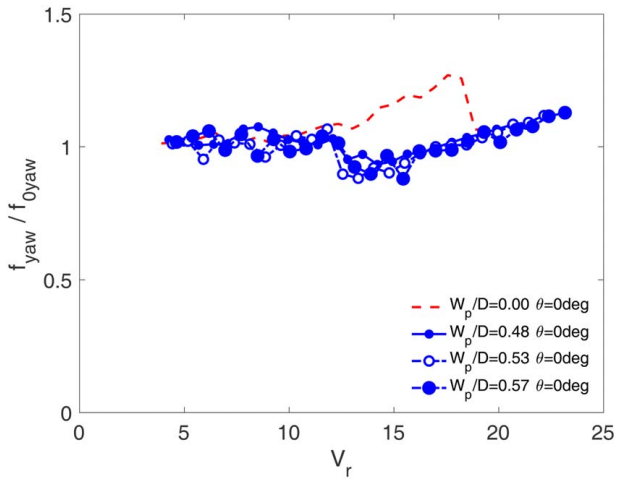

Fig. 14 Non-dimensional frequency for yaw motions for the JPK model with 0-deg incidence and different HP dimensions

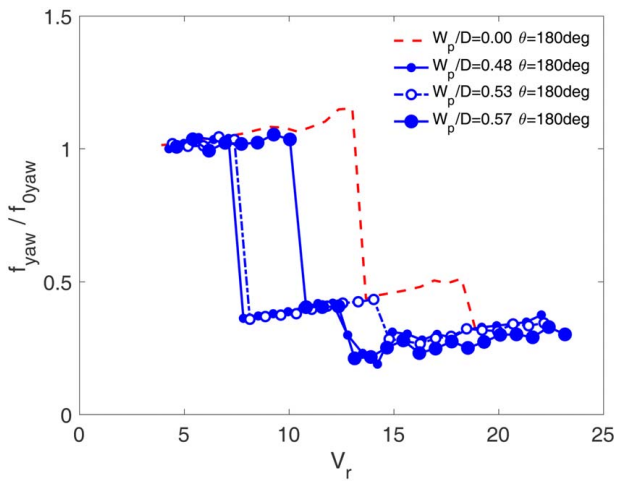

Fig. 15 Non-dimensional frequency for yaw motions for the JPK model with 180-deg incidence and different HP dimensions

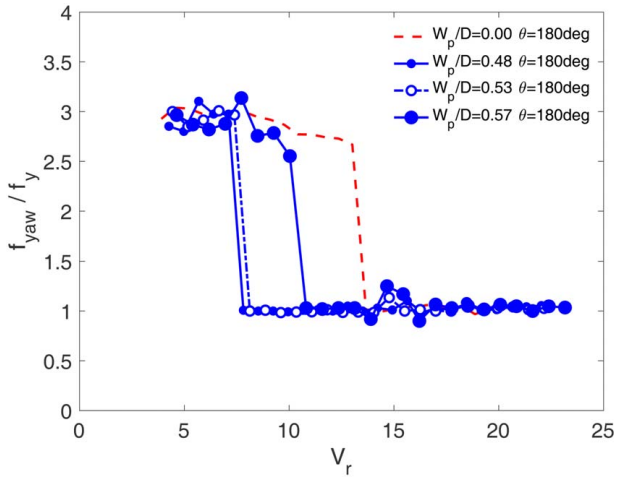

Fig. 16 Non-dimensional ratio of frequency of yaw and motions in the transverse direction for the JPK model with 180-deg incidence and different HP dimensions

When HP was included in the previously discussed cases of the present work, the A_Y/D decreased for both incidences, and again, the lowest amplitudes were observed for the 180-deg incidence. However, for the 180-deg incidence, the OC4 case presented higher transverse amplitudes than the present one without HP, which showed that the central column played an important role. The importance of the central column was confirmed when comparing the same HP conditions for the OC4 and the present work, $W_p/D \sim 0.50$, and the present results showed lower transverse amplitudes.

The results of nominal yaw amplitudes, A_{yaw}, are presented in Figs. 12 and 13 for 0- and 180-deg incidences, respectively. As expected, the highest values of A_{yaw} were observed for the case without HP. The results showed that the presence of HP was responsible for completely mitigating the FIM for this DOF in all conditions with $A_{yaw} < 1$ deg. The case without HP showed a different behavior for 0- and 180-deg incidences, and again, the behavior can be explained by the presence of the central column.

Figures 14 and 15 present the results of the non-dimensional frequency for the yaw motions, f_{yaw}/f_{0yaw}, for 0- and 180-deg incidences, respectively.

For the 0-deg incidence, it was possible to observe a synchronization of the yaw motion with the vortex shedding frequency as shown by the linear behavior of the curve for $V_r > 12$. The behavior matched the linear increase of the yaw amplitudes that may characterize a galloping behavior. The yaw frequency was around the natural frequency of yaw for all reduced velocities.

For the 180-deg incidence, three different behaviors were observed. The first one, $V_r < 10$, was related to small fluctuations of yaw motion around its respective natural frequency. However, for $V_r > 10$, the yaw motion frequencies were the same as the motion frequencies in the transverse direction, as can be confirmed by the ratio between frequencies of yaw and motion in the transverse direction f_{yaw}/f_Y, as in Fig. 16. Therefore, for $V_r > 10$, the mechanism was more complicated than before because we have a coupling between yaw and motions in the transverse direction. Since yaw presented an increase of amplitudes for an increase in the reduced velocity, a galloping or a flutter may occur. More studies must be conducted on these observations since the presence of vortex-induced vibration (VIV) together with galloping and flutter make the problem more complicated.

5 Conclusions

The motivation for the present work was to show the importance of including FIM studies in the design stage of FOWT platforms, particularly the multi-column platform types. The results can be used as a reliable dataset for HP design as a suppression solution of motions due to waves and current incidences.

Flow-induced motions model tests were performed with a 1:60 reduced-scale model in the towing tank of the University of Tokyo, Japan. Two main incidence angles were tested, particularly 0- and 180 deg. For each incidence angle, at least 25 reduced velocities were carried out in the range of $4 < V_r < 25$ and $7,000 < \mathrm{Re} < 50,000$.

Motion characteristic amplitudes for the 6 deg of freedom of motions were measured; transverse and yaw motions were analyzed and discussed in depth.

The presence of the HP is shown to play an essential role in the FIM phenomenon of multi-column platforms, in particular, the JPK model studied.

The presence of HPs decreased the FIM phenomenon, and the impact was more significant the larger the HP dimensions. The phenomenon was mitigated entirely for the largest HP dimension tested, $W_p/D = 0.57$.

The existence of a central column showed that the incidence angle was also an important variable. The presence of a central column was more critical for the 180-deg incidence, whereby an external column downstream was immersed in the wake due to the central column upstream. Results from studies of an array of three cylinders (without a central column) corroborated the statements in this present work. The typical OC4 case geometry was also used as a comparison to highlight the HP and central column effects on the FIM of multi-column systems.

Acknowledgment

This work was developed in the context of the Brazil-Japan collaborative research project n.88887.153223/2017-00 funded by the Brazilian Coordination for the Improvement of Higher Education Personnel (CAPES) and the Japan Society for Promotion of Science (JSPS) and also supported by JSPS KAKENHI Grant No. JP18F18355.

The authors thank the student Matheus A. Marques (Federal University of Pernambuco, Recife, PE, Brazil) for his help during the image development. They also thank Professor Hidetaka Houtani (The University of Tokyo, Tokyo, Japan) for his help during the towing tests assembly.

Conflict of Interest

There are no conflicts of interest.

Data Availability Statement

The data sets generated and supporting the findings of this article are obtainable from the corresponding author upon reasonable request.

Nomenclature

f = frequency of the motion
m = mass
D = characteristic length subjected to vortex shedding or external column diameter
S = distance between external columns
T = draft
U = current velocity
X = inline direction
Y = transverse direction
Z = vertical direction
f_{0n} = natural frequency in still water of nth DOF
f_y = frequency of the motion in the transverse direction

A_Y = characteristic amplitude of the motion in the transverse direction
D_{cc} = diameter of the center column
D_m = diameter of the ring for the mooring line fairleads
D_p = heave plate diameter
D_{pcc} = diameter of the center column heave plate
H_p = heave plate height
H_m = vertical position of the mooring line fairleads
H_t = height of the water level of the towing tank
K_X = total stiffness of the system in the in-line direction
K_{yaw} = total stiffness of the system for the yaw motion
K_Y = total stiffness of the system in the transverse direction
L_m = in-line position of the mooring line fairleads
L_t = length of the towing tank
T_{0n} = natural period of the motion n DOF
V_r = reduced velocity
W_m = transverse position of the mooring line fairleads
W_p = heave plate width
W_t = width of the towing tank
KG = distance between the center of gravity and the base
Re = Reynolds number
St = Strouhal-like number
ζ_n = linear damping ratio of nth DOF
θ = incidence angle
ν = dynamic viscosity

Abbreviations

DD = deep-draft
HP0 = case without HP
HPS = case with a small HP
HPM = case with a medium HP
HPL = case with a large HP
OC4 = Offshore Code Comparison Collaboration

References

[1] Blevins, R. D., 2001, *Flow-Induced Vibration*, 2nd ed., Krieger Publishing Company, Malabar, FL, pp. 104–152.
[2] Zhao, J., Leontini, J. S., Jacono, D. L., and Sheridan, J., 2014, "Fluid–Structure Interaction of a Square Cylinder at Different Angles of Attack," J. Fluid Mech., **747**, pp. 688–721.
[3] Yin, D., Passano, E., Jiang, F., Lie, H., Wu, J., Ye, N., Sævik, S., and Leira, B. J., 2022, "State-of-Art Review of Vortex-Induced Motions of Floating Offshore Wind Turbine Structures," J. Mar. Sci. Eng., **10**(8), p. 1021.
[4] Chen, J., and Kim, C.-H., 2022, "Review of Recent Offshore Wind Turbine Research and Optimization Methodologies in Their Design," J. Mar. Sci. Eng., **10**(1), p. 28.
[5] Liu, Y., Li, S., Yi, Q., and Chen, D., 2016a, "Developments in Semi-Submersible Floating Foundations Supporting Wind Turbines: A Comprehensive Review," Renewable Sustainable Energy Rev., **60**, pp. 433–449.
[6] Lemmer, F., Yu, W., and Cheng, P. W., 2018, "Iterative Frequency-Domain Response of Floating Offshore Wind Turbines With Parametric Drag," J. Mar. Sci. Eng., **6**(4), p. 118.
[7] Suzuki, H., Xiong, J., do Carmo, L. H. S., Vieira, D. P., de Mello, P. C., Malta, E. B., Simos, A. N., Hirabayashi, S., and Gonçalves, R. T., 2019, "Elastic Response of a Light-Weight Floating Support Structure of FOWT With Guywire Supported Tower," J. Mar. Sci. Technol., **24**(4), pp. 1015–1028.
[8] Mello, P. C., Malta, E. B., da Silva, R. O. P., Candido, M. H. O., do Carmo, L. H. S., Alberto, I. F., Franzini, G. R., Simos, A. N., Suzuki, H., and Gonçalves, R. T., 2021, "Influence of Heave Plates on the Dynamics of a Floating Offshore Wind Turbine in Waves," J. Mar. Sci. Technol., **26**(1), pp. 190–200.
[9] Carlson, D. W., and Modarres-Sadeghi, Y., 2017, "Vortex-Induced Vibration of Spar Platforms for Floating Offshore Wind Turbines," Wind Energy, **21**(11), pp. 1169–1176.
[10] Gonçalves, R. T., Chame, M. E. F., Silva, L. S. P., Koop, A., Hirabayashi, S., and Suzuki, H., 2021, "Experimental Flow-Induced Motions (FIM) of a FOWT Semi-submersible Type (OC4 Phase II Floater)," ASME J. Offshore Mech. Arct. Eng., **143**(1), p. 012004.
[11] Robertson, A., Jonkman, J., Masciola, M., Goupee, A., Coulling, A., and Luan, C., 2014, "Definition of the Semi-submersible Floating System for Phase II of OC4," Technical Report No. NREL/TP-5000-60601, National Renewable Energy Lab. (NREL).
[12] Lopez-Pavon, C., and Souto-Iglesias, A., 2015, "Hydrodynamic Coefficients and Pressure Loads on Heave Plates for Semi-submersible Floating Offshore Wind Turbines: A Comparative Analysis Using Large Scale Models," Renewable Energy, **81**, pp. 864–881.
[13] Thiagarajan, K., and Moreno, J., 2020, "Wave Induced Effects on the Hydrodynamic Coefficients of an Oscillating Heave Plate in Offshore Wind Turbines," J. Mar. Sci. Eng, **8**(8), p. 622.
[14] Jiang, Y., Hu, G., Zong, Z., Zou, L., and Jin, G., 2020, "Influence of an Integral Heave Plate on the Dynamic Response of Floating Offshore Wind Turbine Under Operational and Storm Conditions," Energies, **13**(22), p. 6122.
[15] Takata, T., Takaoka, M., Houtani, H., Hara, K., Oh, S., Malta, E. B., Iijima, K., Suzuki, H., and Gonçalves, R. T., 2022, "Effect of Heave Plates on the Wave Motion of a Flexible Multicolumn FOWT," Energies, **15**, p. 7605.
[16] Kosasih, M. A., Suzuki, H., Niizato, H., and Okubo, S., 2020, "Demonstration Experiment and Numerical Simulation Analysis of Full-Scale Barge-Type Floating Offshore Wind Turbine," J. Mar. Sci. Eng., **8**(11), p. 880.
[17] Gonçalves, R. T., Silva, R. O. P., Marques, M. A., Hirabayashi, S., Assi, G. R. S., Simos, A. N., and Suzuki, H., 2020, "Experimental Study on Vortex-Induced Motions of Floating Circular Single Cylinders With Low Aspect Ratio and Different Heave Plate Geometries," Proceedings of the 30th International Ocean and Polar Engineering Conference, Shanghai, China, Aug. 3–7.
[18] Pesce, C. P., Amaral, G. A., and Franzini, G. R., 2018, "Mooring System Stiffness: A General Analytical Formulation with an Application to Floating Offshore Wind Turbines," Proceedings of the ASME 1st International Offshore Wind Technical Conference, IOWTC2018-1040, San Francisco, CA, Nov. 4–7.
[19] Assi, G. R. S., 2014, "Wake-Induced Vibration of Tandem Cylinders of Different Diameters," J. Fluids Struct., **50**, pp. 329–339.
[20] Gonçalves, R. T., Meneghini, J. R., and Fujarra, A. L. C., 2018d, "Vortex-Induced Vibration of Floating Circular Cylinders With Very Low Aspect Ratio," Ocean Eng., **154**, pp. 234–251.
[21] Gonçalves, R. T., Hannes, N. H., Chame, M. E. F., Lopes, P. P. S. P., Hirabayashi, S., and Suzuki, H., 2020, "FIM—Flow-Induced Motions of Four-Column Platforms," Appl. Ocean Res., **95**, p. 102019.
[22] Gonçalves, R. T., Chame, M. E. F., Hannes, N. H., Lopes, P. P. S. P., Hirabayashi, S., and Suzuki, H., 2020, "FIM—Flow-Induced Motion of Three-Column Platforms," Int. J. Offshore Polar Eng., **30**(2), pp. 177–185.